Catalysis Today 273 (2016) 3–11

Contents lists available at ScienceDirect

Catalysis Today

journal homepage: www.elsevier.com/locate/cattod

Preparation of structured catalysts with Ni and Ni–Rh/CeO_2 catalytic layers for syngas production by biogas reforming processes

C. Italiano [a,*], R. Balzarotti [b], A. Vita [a], S. Latorrata [b], C. Fabiano [a,c], L. Pino [a], C. Cristiani [b]

[a] Institute CNR-ITAE, Via Salita S. Lucia sopra Contesse n. 5, S. Lucia, 98126 Messina, Italy
[b] Politecnico di Milano, Dipartimento di Chimica, Materiali e Ingegneria Chimica "G. Natta", Piazza Leonardo da Vinci 32, 20133 Milano, Italy
[c] Università degli Studi "Mediterranea" di Reggio Calabria, Dipartimento di Ingegneria Civile, dell'Energia, dell'Ambiente e dei Materiali, Salita Melissari, 89124 Reggio Calabria, Italy

ARTICLE INFO

Article history:
Received 27 November 2015
Received in revised form 25 January 2016
Accepted 29 January 2016
Available online 11 February 2016

Keywords:
Structured supports
Monoliths
Foams
Washcoating
Steam reforming
Oxy-steam reforming
Nickel
Rhodium
Bimetallic catalyst

ABSTRACT

Ni(7.5 wt.%)/CeO_2 and Ni(7.5 wt.%)-Rh(0.5 wt.%)/CeO_2 powders (previously prepared by solution combustion synthesis) were washcoated on cordierite monolith and alumina open-cell foam by means of support dip-coating into acid-free catalyst dispersion. Catalytic performances toward the steam reforming (SR) and the oxy-steam reforming (OSR) of biogas were investigated and compared at different temperatures (700–800 °C) and weight space velocities (WSV = 70,000–350,000 Nml g_{cat}^{-1} h^{-1}). Coating load was controlled by multiple depositions; homogeneous and well adherent layers were found. Catalytic tests demonstrated superior performances of the bimetallic samples (Ni–Rh/CeO_2) compared to the monometallic one (Ni/CeO_2), especially at high space velocity. At the same time, foam showed better performances with respect to the monolithic support toward the SR and OSR processes.

1. Introduction

Successive crises in energy and global warming have been increased the study for more efficient technologies and renewable sources of electricity generation [1]. In this context, fuel cells have been developed in the last decades for transportation, as well as for both stationary and portable power generation [2]. Fuel cells, operating using hydrogen or hydrogen-rich fuels (syngas), can potentially contribute to increase distributed energy generation and to reduce pollutants emissions into the environment [3–5]. At present, the commercial production of hydrogen is mostly based on steam reforming of fossil fuels [6]. However, from the standpoint of fossil fuels limitations and also global climate changes, alternative ways are under investigation in order to replace fossil hydrocarbons with renewable sources, such as biogas [7,8]. Thus, reforming technologies (principally Steam Reforming (SR) and Oxy Steam Reforming (OSR)) of biogas for hydrogen/syngas production will play a crucial role in the transition to the "hydrogen based economy" [1,6,9–11].

Biogas reforming catalysts range from noble metals (Rh, Ru, Pt, Pd Ir) [12–15] to base metals (Ni, Co) supported over metal oxides, mixed oxides and perovskites [16–18]. Particular attention is devoted to the development of non-noble metal catalysts, due to high cost and limited availability of noble metals. Nickel-based catalysts are the most investigated catalytic systems despite they may be quickly deactivated by sintering and coking phenomena [19]. Redox support materials, such as ceria-based solid solutions or mixed oxides, have been reported to prevent metal sintering, due to strong metal-support interactions (SMSI). Moreover, they are generally employed to mitigate catalyst deactivation by carbon deposition, due to oxygen storage capabilities [18,19]. In our previous works, it was reported that Ni/CeO_2 catalysts showed high catalytic performance in OSR of biogas [19,20]. The other way to improve catalyst anti-coking property is to introduce a second metal component to form a bimetallic catalyst system [6,9,21]. Several authors reported that a small noble metal addition (Rh, Pt or Pd) can improve catalyst stability [9,21,22]. Among the preparation procedures, Solution Combustion Synthesis (SCS) provides an attractive practical alternative to the conventional preparation methods since it is simple, low-cost, saving in time and energy consumption [23–25], resulting in nanocrystalline oxide

* Corresponding author. Fax: +39090624247.
E-mail address: cristina.italiano@itae.cnr.it (C. Italiano).

http://dx.doi.org/10.1016/j.cattod.2016.01.037
0920-5861/

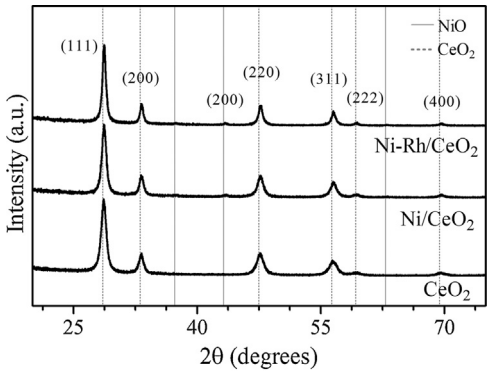

Fig. 1. XRD spectra of synthesized CeO_2, Ni/CeO_2 and $Ni–Rh/CeO_2$ powders.

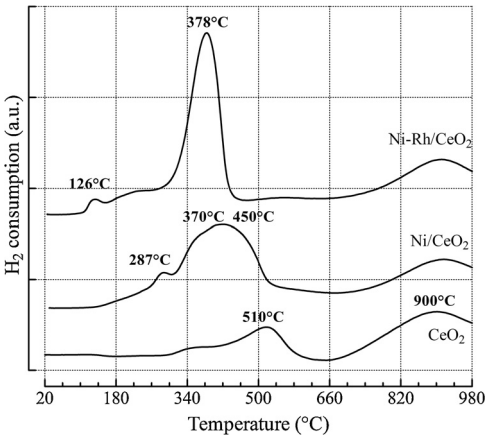

Fig. 2. H_2-TPR patterns of CeO_2, Ni/CeO_2 and $Ni–Rh/CeO_2$ powders.

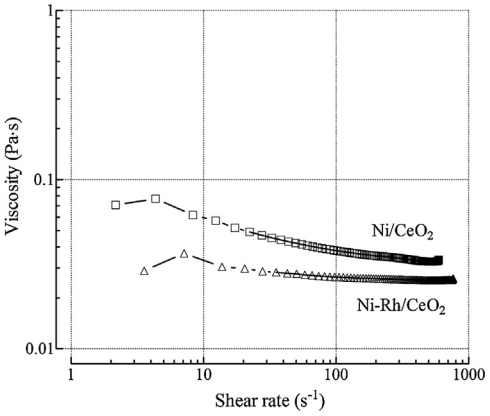

Fig. 3. Rheological properties of catalytic HGP-based slurries.

powders production with increased homogeneity and reduced size [18,20,26].

Structured catalysts with active components supported on ceramic honeycombs [27–29] and foams [29–32] are well-known to have many advantages, providing an efficient heat and mass transfer compared to conventional packed bed reactors. Good thermal conductivity is especially important in the case of energy-intensive processes to prevent emergence of hot spots/cool zones within the reactor, that could result in a deterioration of catalysts performance [33,34]. Among the many methods available [35], dip-coating into a solution or a dispersion is widely considered the best procedure in order to washcoat geometrical supports [36–39]. Dip-coating process is based on the immersion of the morphological substrate into a slurry containing the catalytic active phase. Once substrates voids are filled, the withdrawing process allows to create an homogeneous film on support surface, thanks to the balance between the gravitational force, attracting the film downward, and the viscous force, which hinders its sliding [40]. On these bases, theological behavior and withdrawal speed are the most important parameters to be tuned in order to properly control coating layer formation [41]. Slurry rheological behavior depends on a large variety of variables, both from the formulation components (binder, dispersant, solvent) and powder properties (properly sized powder, nature of suspended solids) points of view. All those parameters directly influence viscosity, which is strictly connected to wash-coat load/thickness and adhesion properties [41,42]. Suspension stabilization is often achieved by using a water-based acidic solution that allows particle repulsion by means of surface charging [42–44]. Unfortunately, this method shows some limitations as, in some case, an acidic solution may induce significant changes on both chemical and morphological catalyst properties [45].

In this work, Ni/CeO_2 and $Ni–Rh/CeO_2$ powders (previously prepared by SCS) were washcoated on cordierite monoliths (500 cpsi, diameter 1 cm, length 1.5 cm) and alumina foams (30 ppi, diameter 1 cm, length 1.5 cm) by means of support dip-coating into acid-free catalyst dispersion. Polyvinyl alcohol was used both as rheology modifier and binder: the dependence of coating load, homogeneity and adhesion was evaluated with respect to rheological properties and multiple dip-coating depositions. The catalytic performances of the obtained structured catalysts were investigated toward biogas steam reforming (SR) and oxy-steam reforming (OSR) reactions.

2. Experimental

2.1. Catalyst preparation and characterization

$Ni(7.5\,wt.\%)/CeO_2$ and $Ni(7.5\,wt.\%)Rh(0.5\,wt.\%)/CeO_2$ catalysts were prepared by the Solution Combustion Synthesis method (SCS), according to a procedure that was described elsewhere [18,20]. In a typical experiment, stoichiometric amounts of Ce precursor ($Ce(NO_3)_3{\cdot}6H_2O$ from Alfa Aesar), Ni precursor ($Ni(NO_3)_2{\cdot}6H_2O$ from Sigma–Aldrich) and Rh precursor ($RhCl_3{\cdot}xH_2O$ from Sigma–Aldrich) were dissolved in the minimum quantity of distilled water (~100 ml) with the suitable quantity of fuel (urea, CH_4N_2O from Sigma–Aldrich). The amount of fuel was determined by the so-called fuel-to-oxidant ratio and it was calculated using the total oxidizing (O) and reducing (F) valences of the components in order to have an equivalence ratio equal to 1 ($\phi = O:F = 1$); the latter corresponds to a maximum release of energy. The obtained solution was introduced into a preheated muffle furnace (350 °C). In the beginning the solution boils, foams and then undergoes intense flaming combustion with evolution of gases (N_2, CO_2 and H_2O), yielding a very voluminous powder. The resulting powders were calcined at 600 °C for 2 h (heating rate set at 5 °C min^{-1}) to eliminate combustion carbon residues. The Ni and Rh content in the catalytic powders was confirmed by chemical analysis (ICP/OES).

Specific surface area was estimated from adsorption/desorption isotherms at liquid nitrogen temperature (−196 °C) on *Micromeritics ASAP 2020* instrument and it was calculated according to the Brunauer–Emmet–Teller (BET) equation.

X-ray diffraction (XRD) analysis of the synthesized catalysts was conducted using a *Philips X-Pert 3710* diffractometer that was equipped with a Cu Kα radiation at 40 kV and 20 mA. X-ray diffraction patterns were recorded in the scan ranges of $2\theta = 20–75°$ (1.50°/min), $2\theta = 27–30°$ (0.06°/min) and $2\theta = 42–45°$ (0.06°/min). The crystallite size was calculated using Scherrer equation, by using the most intense observed reflection for NiO (2 0 0) and CeO_2 (1 1 1)

crystallographic structures, respectively. CeO_2 lattice parameter (α) was obtained from the related pattern at low scan rate.

Catalyst reducibility was studied by H_2 Temperature Programmed Reduction (TPR) using a *Micromeritics ChemiSorb 2750* instrument. A continuous flow of 5% H_2/Ar (30 NmL/min) was passed over the catalyst and temperature was raised up to 1000 °C with a 20 °C/min rate. Before measurements, all catalyst samples were treated in situ at 500 °C for 30 min under O_2 flow. The H_2 consumption was monitored by a thermal conductivity detector (TCD) and the response was quantitatively calibrated from the TPR area of known amounts of CuO. The degree of reduction of CeO_2, NiO and Rh_2O_3 was calculated by taking the ratio of actual H_2 consumption to theoretical H_2 requirement to reduce all the metal oxides present in the sample, by assuming constant degree of reduction of support material.

2.2. Washcoating procedure

Catalyst powders (Ni/CeO_2 and NiRh/CeO_2) were washcoated on both cordierite monolith and alumina open cell foam. Monoliths (500 cpsi, diameter 1 cm, length 1.5 cm) were supplied by Chauger Honeycomb Ceramics (Taiwan), while foams (30 ppi, diameter 1 cm, length 1.5 cm) were provided by Lanik company (Czech Republic). Powders dispersions were obtained according to a procedure reported elsewhere [43,44]. Glycerol (87% w/w water solution, Sigma–Aldrich) was used as dispersant and distilled water was used as solvent/diluent. Glycerol/powder ratio of 1.9 and water/powder ratio of 1.5 were used, respectively. 2 wt.% of polyvinyl alcohol (PVA) (Mowiol from Sigma–Aldrich) related to water–glycerol mixture was used as rheology modifier. In a typical experiment, the dispersion medium (HGP) was produced by dissolving PVA in distilled water and then by adding glycerol under magnetic stirring at 85 °C. Catalyst powder was thus added to the HGP medium and the resulting slurry was ball-milled using ZrO_2 spheres (1 cm diameter and mass ratio with respect to powder equal to 7) as grinding bodies for 24 h at 50 rpm in a polyethylene jar. At the end of milling process, a sonication treatment was performed for 30 min on the slurry in order to reduce foaming. A dynamic stress device (*Rheometrics*) was used to assess slurry rheological properties. Parallel disc plate geometry (40 mm diameter) was chosen; dynamic viscosity was evaluated in the 1–10^3 s^{-1} shear rate range at 25 °C. Structured supports were washed in acetone by ultrasound bath for 30 min before deposition process. Slurry deposition was carried out by dip-coating, at constant withdrawal rate of 13 cm min^{-1} for both dipping and withdrawal steps. Multiple dippings were performed in order to obtain a coating load of 15–20 wt.%. After each dipping, samples were flash dried in air for 6 min at 350 °C in a sealed oven. In order to obtain the final coated catalysts, a 10 h calcination process was performed at 800 °C (2 °C min^{-1} heating rate).

Gravimetric analysis was performed after each flash drying step and after the final calcination process, in order to control weight evolution and to assess washcoat load. Final washcoat load was determined by weight, as difference between the bare and the coated support.

Coating adhesion was determined by sonication for 30 min in petroleum ether bath, according to literature [43,44].

SEM investigation of structured catalysts was obtained using a *FEI XL 30* microscope that was equipped with a field emission gun. Optical microscope (*Olympus, SZ-CTV microscope*) was used to assess coating homogeneity.

In the following, the obtained structured systems will be identified as Ni–MO, NiRh–MO, Ni–FO and NiRh–FO as a function of the catalytic formulation (Rh and NiRh for Ni/CeO_2 and NiRh/CeO_2 catalysts, respectively) and the support (MO and FO for monolith and foam, respectively).

2.3. Catalytic tests

Biogas SR and OSR experiments were carried out in a quartz fixed-bed reactor (i.d.=1 cm) that is inserted into a PID temperature controlled furnace. Prior to reaction, structured catalysts were reduced by 50% H_2/N_2 stream (30 NmL/min) at 450 °C for 1 h. Then, catalytic performance was studied feeding a mixture of methane, carbon dioxide, steam and/or oxygen. SR experiments were conducted feeding reagents with CH_4:CO_2:H_2O:N_2 = 1.0:0.67:3.0:0.2 molar ratios, while OSR experiments were carried out at CH_4:CO_2:H_2O:O_2:N_2 = 1.0:0.67:0.3:0.1:0.1 molar ratios. High purity gases (99.999%, from RIVOIRA) were used in the experiments, keeping constant flow rates by using mass flow-controllers (*Brooks Instrument Smart Mass Flow*). Steam was fed using an isocratic pump (Agilent 1100 Series) and a specially designed evaporator. Tests were carried out varying temperature (700–800 °C) and weight space velocity (WSV = 70,000–350,000 Nml g_{cat}^{-1} h^{-1}), defined as volumetric flow rate of the reactants at 0 °C and 1 bar per gram of catalytic layer. Reaction temperature (T_{SET}) was measured at the center of catalyst bed, between the catalytic system and the tubular quartz reactor, using a chromel/alumel thermocouple. Moreover, two thermocouples were positioned at the inlet (T_{IN}) and at the outlet (T_{OUT}) of the catalytic bed respectively to measure the temperature gradient that is generated by reactions. The duration of each test was set to 6 h. Reagents and products compositions were determined using an on-line gas chromatograph (*Agilent 6890 Plus*) that was equipped with thermal conductivity (TCD) and flame ionization (FID) detectors. CH_4, which was revealed in both detectors, was used as reference compound, while N_2 was used as internal standard for mass balance calibration.

The experimental results were compared with the thermodynamic equilibrium values calculated by a commercial steady state simulation package named Aspen Plus® by AspenTech, based on the minimization of Gibbs free-energy of each of the existing species (CH_4, O_2, H_2O, CO_2, CO, H_2, solid carbon). The calculation was carried out at the reaction temperature (T_{SET}) and at the maximum temperature recorded at the outlet (T_{OUT}) of the catalytic bed [34].

3. Results and discussion

3.1. Catalyst characterization

The main textural and structural characteristics of the synthesized Ni/CeO_2 and Ni–Rh/CeO_2 catalysts are included in Table 1 and they are compared with those of CeO_2 carrier that was prepared by the same route. The synthesized powders exhibited specific surface area varying in the range of 10–15 m^2/g. XRD patterns of the systems are shown in Fig. 1. All systems were characterized by a typical cubic fluorite structure of ceria, corresponding to the (1 1 1), (2 0 0), (2 2 0), (311), (2 2 2) and (4 0 0) planes (reference JCPDS 4–593). The average particle size of the samples, that was calculated by Scherrer equation (Table 1), indicated a particles size of 10.9 nm for the CeO_2 carrier, that slightly increased to 13.1 and 16.9 nm for Ni/CeO_2 and Ni–Rh/CeO_2 catalysts, respectively. No clear evidence of Ni active phase can be noticed; this is a signal of the presence of small and well distributed particles. However, the small reflection at 2θ = 43.33° could be attributed to the presence of nickel oxide (reference JCPDS 4–835), which corresponds to NiO particles size of ca. 13.1 and 17.8 nm. Besides, rhodium identification is probably hampered in view of its small amount, that falls below the detection limit. In addition, the lattice contraction (5.385–5.387 Å compared to 5.394 of CeO_2) indicated the partial incorporation of smaller Ni^{2+} ions ($r_{Ni^{2+}}$ = 0.81Å) and probably of Rh^{3+} ions ($r_{Rh^{3+}}$ = 0.68Å) into the lattice of ceria Ce^{4+} ($r_{Ce^{4+}}$ = 0.97Å) to form a solid solution [46].

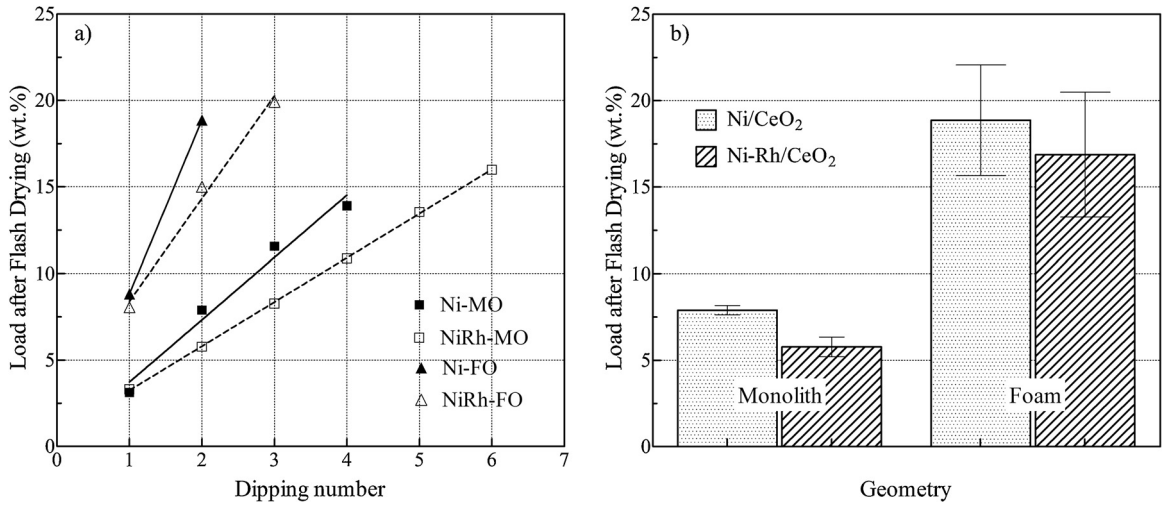

Fig. 4. Washcoat load evolution (a) after flash drying (a) as function of the dipping number and (b) after two dippings. Effect of catalytic sample and support geometry.

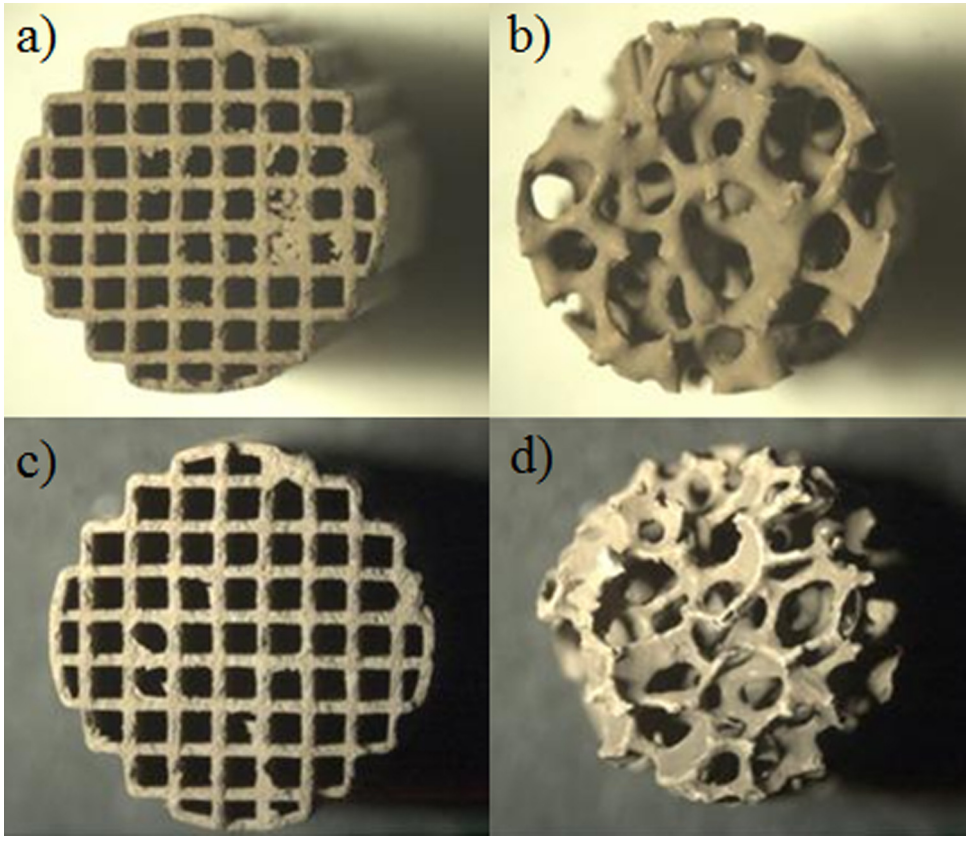

Fig. 5. Optical microscope characterization of Ni/CeO_2 based samples (top, a–b) and $Ni–Rh/CeO_2$ based samples (bottom c–d) supported on monolith (right) and foam (left).

Table 1
Main textural and structural properties of synthesized CeO_2, Ni/CeO_2 and $Ni–Rh/CeO_2$ powders.

Sample	BET Surface area (m^2/g)	X-ray		
		CeO_2 size[a] (nm)	CeO_2 lattice parameter[a] (Å)	NiO size[a] (nm)
CeO_2	15	10.9	5.394	–
Ni/CeO_2	11	13.1	5.387	11.7
$Ni–Rh/CeO_2$	10	16.9	5.385	17.8

[a] Calculated from X-ray diffraction: CeO_2 particle size from the Scherrer's equation of the CeO_2 (111) reflection; lattice parameter (α) from the relation $\alpha = \sqrt{h^2 \times k^2 \times l^2}(\lambda/2 \times \sin\theta)$.

Table 2
Geometric properties of bare supports (monolith and foam).

Sample	Characteristics size $d_{p(mm)}$	Wall/Strut thickness t (mm)	Bed density (kg/m^3)	Bed porosity (%)	Open frontal area ε	Geometric surface area GSA (m^2/m^3)
Cordierite monolith	0.83	0.32	771	72.5	0.52	2529
Alumina foam	1.40	0.43	383	83.6	0.86	988

Fig. 2 compares the H_2-TPR profiles of the CeO_2 carrier and the Ni/CeO_2 and Ni–Rh/CeO_2 catalysts. For bare ceria, two main reduction peaks were observed, at 510 and 900 °C, respectively. As reported in literature, the low-temperature peak is due to the reduction of CeO_2 surface oxygen, while the high-temperature peak is due to CeO_2 bulk oxygen reduction [46,47]. The amount of hydrogen consumption of low-temperature peak (510 °C) was 0.6 mmolH_2/g_{cat}, which corresponds to ca. 10% of the reducible CeO_2 species. The catalyst containing Ni showed reduction peaks at 287, 370, 450 and 900 °C, as previously reported [18,20,46]. The low-temperature zone (temperatures range between 130 and 300 °C with a maximum at ca. 287 °C) is ascribed to adsorbed oxygen reduction due to NiO solid solution formation into CeO_2 [46,48,49]. Besides, the contribution of bulk NiO particles reduction without interaction with the ceria support cannot be excluded [50]. In the middle-temperature zone, the peak at 370 °C can be correlated to the reduction of NiO interacting with (but not chemically bound to) the support, while the latter peak (at 450 °C) can be associated to the formation of Ni–Ce solid solution [20,50] and to the reduction of CeO_2 surface oxygen, shifted towards lower temperature than the bare ceria (510 °C) due to the effect of Ni. The high-temperature zone is ascribed to CeO_2 bulk oxygen reduction, which does not seem affected by Ni presence [50,51]. The amount of hydrogen consumed by NiO species at 287, 370 and 450 °C, was 1.2 mmolH_2/g_{cat}, corresponding to a reduction degree of ca. 95%. However, a partial contribution due to the reduction of CeO_2 to Ce_3O_4 cannot be excluded. The catalyst containing both Rh and Ni exhibited a rearrangement of the reduction profile, with two main peaks at 126 °C and 378 °C, which can be ascribed to Rh_2O_3 and NiO reduction, respectively. Similar profile has been reported by Kugai et al. [51]. The degree of reduction of Rh_2O_3 and NiO species was 74 and 96%, respectively, but even in this case it is difficult to estimate the contribution of CeO_2 species reduction. Indeed, surface ceria reduction was facilitated, via hydrogen spillover, by the presence of Rh; hydrogen, after dissociation on metallic Rh, was able to spill over to CeO_2 and to reduced it at lower temperatures, as evidenced by Hou et al. [49].

According to the procedure described in the experimental section, catalyst powders were dispersed in the HGP liquid medium and their rheological behavior was assessed. Results are reported in Fig. 3. Ni/CeO_2 slurry displayed a lightly shear thinning behavior, with a viscosity value of 0.059 Pa s in the typical shear range for dip-coating applications (i.e. about 10 s^{-1}). The addition of rhodium induced some changes on rheological behavior: viscosity decreased down to 0.033 Pa s (at 10 s^{-1}) and the flow curve displayed a quasi-Newtonian behavior, especially at high shear rate values. These small differences could be due to the diverse volume fraction of the powder used for preparing the slurry; in particular, a lower volumetric fraction was used in the case of Ni–Rh/CeO_2 catalyst, due to the presence of heavier rhodium ions.

3.2. Support washcoating

Ni/CeO_2 and Ni–Rh/CeO_2 slurries were deposited on both ceramic monoliths and open cell foams, according to the procedure reported in Section 2.2. The main geometrical characteristics of bare supports are listed in Table 2. The characteristic sizes (d_p) are the channel inner size (monolith) and the pore diameter (foam) [52]. Monolith channel inner size (d_p) and wall thickness (t) were microscopically determined by using 30 different supports. Foam pore diameter (d_p) and strut thickness (t) were microscopically determined by using ca. 500 features of 30 different supports. Bed density was calculated by using bed weight and volume. Bed porosity was determined by helium pycnometry. The open frontal area (ε) of monolithic support was calculated from channel inner size (d_p) and wall thickness (t) by equation $\varepsilon = {d_p}^2/\left(d_p + t\right)^2$ [53]. Foam open frontal area was calculated from the relative density (ρ_A/ρ_B) by the equation $\varepsilon = 1 - \rho_A/\rho_B = 1 - \left[2.59 \times (t/t + d_p)^2\right]$ [54]. Monolith geometric surface area (GSA) was calculated according to Cybulski and Moulijn [55], while the tetrakaidecahedron model of Buciuman and Kraushaar-Czarnetzki [56] was used for the foam.

Results in terms of washcoat load after flash drying as a function of dipping number are reported in Fig. 4a. A linear trend between coating load and dipping number was clearly manifest in both samples. From the observation of the load-dipping curves, also a good washcoat process reproducibility was detected: almost the same coating load was deposited after each dipping step. Washcoat load appears to be dependent on the complexity of the structured supports. As a matter of fact, honeycomb monoliths, that have straight and parallel channels, display always a lower washcoat load with respect to foams. Indeed, after two dippings, foam coating amount was almost twice the load of the monolith; this behavior can be ascribed to the surface area per unit volume (GSA), which is higher in ceramic foam than in monolith (Table 2). Not surprisingly, also the rheological behavior influences washcoat load: higher loads were obtained by using Ni/CeO_2 slurry, that is the sample with the highest slurry viscosity. These behaviors are better clarified in Fig. 4b, where the average load after two dippings is reported as a function of support geometry and catalytic formulation. Indeed, the final coating load can be managed with a multiple-dipping process up to the final load required for the application. In this case, the final washcoat of 15–20 wt.% was reached after 2–6 dipping steps, depending on the sample, or more precisely on the slurry rheological behavior, and on the support geometry. In addition, washcoat load was evaluated dividing coating mass by morphological support surface area. For both systems (i.e. MO and FO), washcoat load with respect to morphological support surface area unit was found to be ca. 0.06 g/cm^2. This is a first indication of the fact that, regardless structured support shape, similar washcoat layers thickness are expected. Fig. 5 shows the images of the structured systems obtained by means of optical microscope. In all cases, very good washcoat homogeneity was found. Honeycomb channels as well as foam pores were almost open and no pore clogging was detected. Therefore, the slurry was only deposited onto the external surface, as a "skin layer" of the geometrical support.

Adhesion tests results pointed out sufficiently good coated layers adhesion, with average losses of 25 wt.% and 18 wt.% for Ni/CeO_2 and Ni–Rh/CeO_2 samples respectively, in case of washcoat on foam supports. Better results were obtained for monolithic supports, that are characterized by losses lower than 10 wt.%. Weight losses are referred to washcoat load before and after the tests and they are in line with results obtained for other geometrical supports and similar washcoat compositions [29,37,38]. It has to be considered that ultrasound tests are particularly stronger if compared to the stresses experienced by washcoat inside a reactor [35,38].

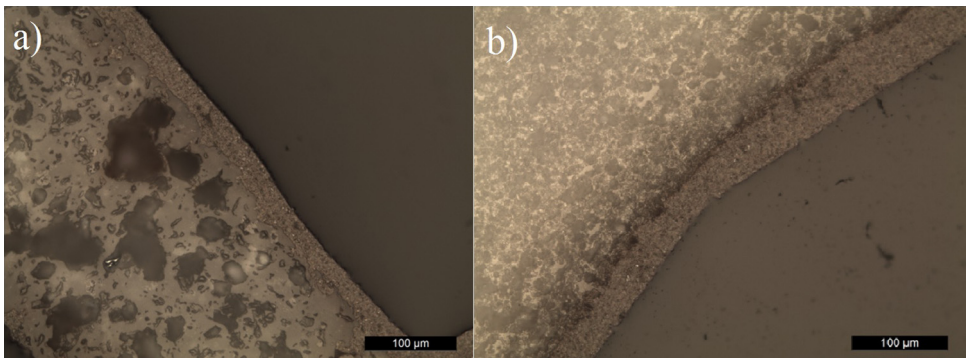

Fig. 6. SEM analysis of NiRh–MO (a) and NiRh–FO (b) coating thickness.

Table 3
Biogas SR activity results on Ni/CeO_2 and $Ni–Rh/CeO_2$ catalysts washcoated on monolith and foam at different temperature (700–800 °C) and space velocity (WSV = 250,000–350,000 Nml g_{cat}^{-1} h^{-1}).

Catalyst	WSV (Nml g_{cat}^{-1} h^{-1})	T_{SET} (°C)	T_{IN} (°C)	T_{OUT} (°C)	χ_{CH4} (%)	χ_{CO2} (%)	H_2/CO	Products composition (%)*			
								CH_4	CO_2	H_2	CO
Ni–MO	250,000	800	883	904	97.6	−3.0	3.13	0.53	14.63	64.28	20.56
	350,000	800	902	879	97.3	−4.4	3.18	0.59	14.96	64.24	20.21
NiRh–MO	250,000	800	801	822	99.9	−2.1	3.12	0.02	14.82	64.51	20.65
	350,000	800	804	822	99.9	−3.5	3.12	0.03	14.81	64.47	20.69
NiRh–FO	250,000	800	806	825	99.9	−1.9	3.06	0.03	14.58	64.38	21.01
	350,000	800	824	839	99.9	−1.4	3.08	0.02	14.65	64.41	20.92
Ni–MO	250,000	700	785	795	83.1	−29.0	4.14	3.90	19.29	61.86	14.95
	350,000	700	806	770	77.2	−27.1	4.13	5.59	20.23	59.72	14.46
NiRh–MO	250,000	700	712	729	96.7	−21.9	3.71	0.70	17.26	64.62	17.42
	350,000	700	716	723	92.3	−20.8	3.70	1.65	17.77	63.44	17.14
NiRh–FO	250,000	700	713	725	98.6	−19.1	3.60	0.29	16.90	64.81	18.00
	350,000	700	727	731	98.6	−19.3	3.63	0.30	16.93	64.91	17.86

* Dry and N_2-free basis.

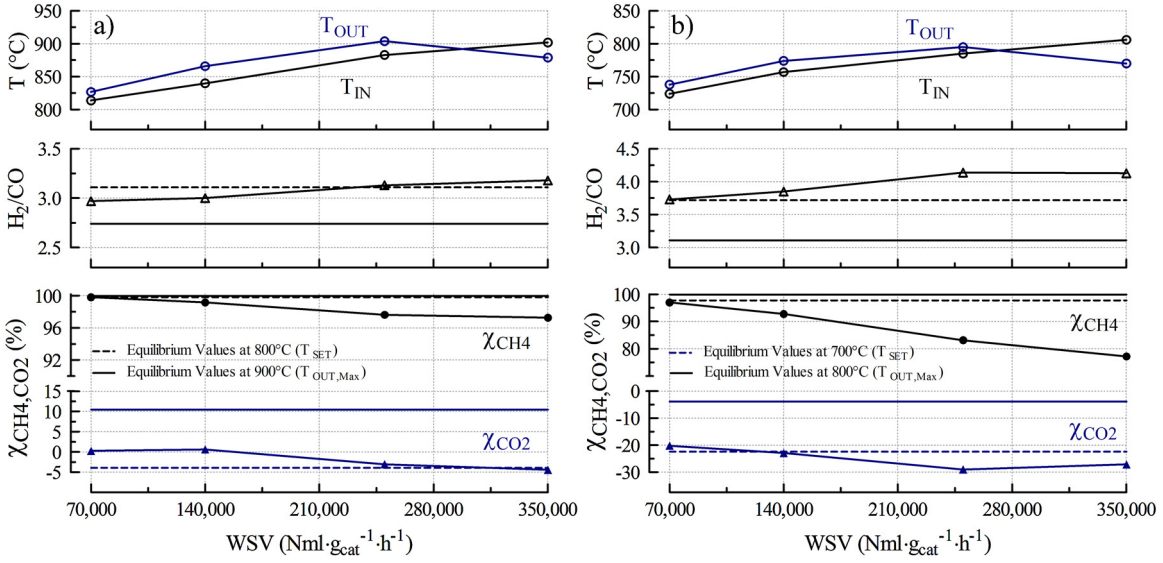

Fig. 7. Biogas SR activity results on Ni/CeO_2 catalyst washcoated on monolith: effect of space velocity (WSV = 70,000–350,000 Nml g_{cat}^{-1} h^{-1}) at 800 (a) and 700 °C (b).

Coating thickness was evaluated by SEM measurements, resulting ca. 20–30 μm, as reported in Fig. 6 for NiRh–MO and NiRh–FO systems.

3.3. Activity tests

3.3.1. SR and OSR activity of Ni/CeO_2 on monoliths

Ni-MO catalyst performance was first evaluated in SR reaction of biogas at atmospheric pressure and H_2O/CH_4 ratio of 3. The effect of weight space velocity (WSV = 70,000–350,000 Nml g_{cat}^{-1} h^{-1}) at different temperatures (700–800 °C) was addressed and results are shown in Fig. 7 in terms of methane (χ_{CH4}) and carbon dioxide (χ_{CO2}) conversion and H_2/CO molar ratio. Recorded temperatures at the inlet (T_{IN}) and at the outlet (T_{OUT}) of the catalytic bed are also reported. At the WSV of 70,000 Nml g_{cat}^{-1} h^{-1}, CH_4 conversion approached equilibrium values at both investigated temperatures (T_{SET}, 800–700 °C, at the center of the catalytic bed). CO_2 conversions were found to be slight higher than the equilibrium values

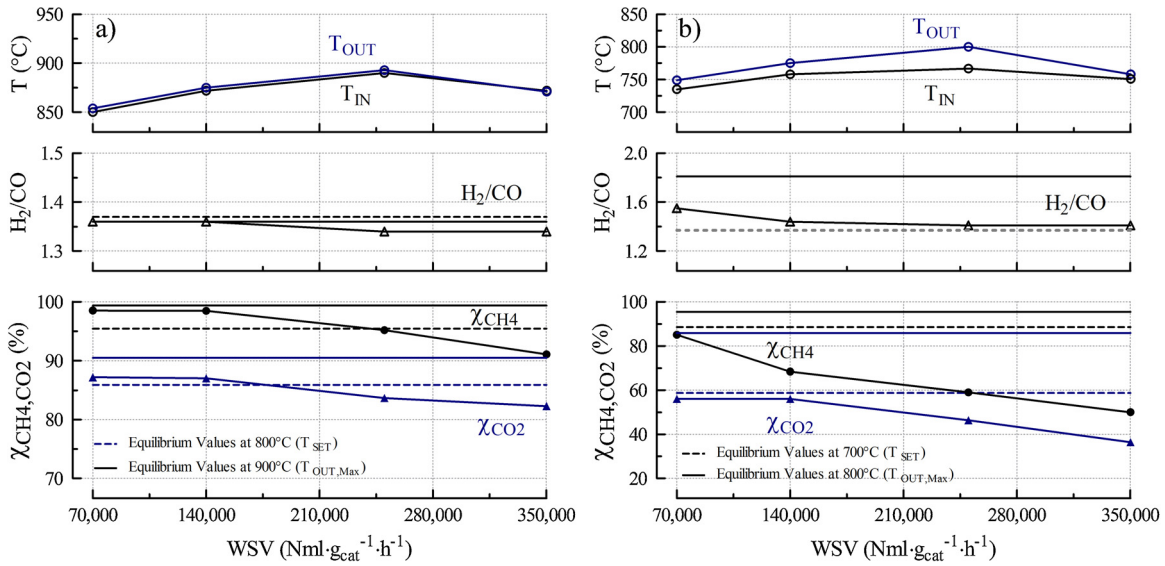

Fig. 8. Biogas OSR activity results on Ni/CeO_2 catalyst washcoated on monolith: effect of space velocity (WSV = 70,000–350,000 Nml g_{cat}^{-1} h^{-1}) at 800 (a) and 700 °C (b).

Table 4
Biogas OSR activity results on Ni/CeO_2 and $NiRh/CeO_2$ catalysts washcoated on monolith and foam at different temperature (700–800 °C) and space velocity (WSV = 250,000–350,000 Nml g_{cat}^{-1} h^{-1}).

Catalyst	WSV (Nml g_{cat}^{-1} h^{-1})	T_{SET} (°C)	T_{IN} (°C)	T_{OUT} (°C)	χ_{CH4} (%)	χ_{CO2} (%)	H_2/CO	Product composition (%)*			
								CH_4	CO_2	H_2	CO
Ni–MO	250,000	800	890	893	95.2	83.7	1.34	1.24	3.11	54.80	40.85
	350,000	800	872	871	91.1	82.3	1.34	2.34	3.27	54.06	40.33
NiRh–MO	250,000	800	867	869	95.8	85.5	1.37	1.07	2.63	55.69	40.61
	350,000	800	872	873	92.1	83.6	1.37	2.06	3.01	54.89	40.04
NiRh–FO	250,000	800	846	848	96.8	87.3	1.36	0.83	2.27	55.88	41.02
	350,000	800	864	864	94.7	84.2	1.37	1.38	2.91	55.41	40.30
Ni–MO	250,000	700	800	767	59.0	46.4	1.43	14.73	12.54	42.81	29.92
	350,000	700	758	751	50.0	36.4	1.41	19.49	16.29	37.58	26.64
NiRh–MO	250,000	700	753	742	73.3	61.7	1.34	7.99	8.29	47.95	35.77
	350,000	700	770	748	65.4	55.3	1.34	11.12	10.13	45.12	33.63
NiRh–FO	250,000	700	738	726	77.4	66.9	1.36	6.74	6.83	49.85	36.58
	350,000	700	749	726	69.0	56.4	1.35	9.90	9.80	46.19	34.11

* Dry and N_2-free basis.

calculated at reaction temperatures. This could be due to the measured T_{IN} and T_{OUT} that were always higher than T_{SET} and that were probably affected by the heat transferred from the furnace to the catalytic bed, which supports the endothermic steam reforming reaction [20,34,35]. Increasing the WSV, catalytic performances decreased as was expected, in terms of both CH_4 (from 99.8 to 97.3 at 800 °C) and CO_2 conversion. The decrease in catalytic activity was more pronounced at low temperature (700 °C), where methane conversion decreased from 97.0 to 77.2%. Moreover, CO_2 was produced by SR and water gas shift (WGS) reactions, that are both favored by the high steam content in the reactants stream (S/C = 3.0), resulting in low CO_2 conversion [57].

Fig. 8 shows the effect of WSV at 800 (Fig. 8a) and 700 °C (Fig. 8b) on Ni–MO catalytic activity towards the OSR reaction. A reactant mixture poor in steam and oxygen (S/C and O_2/C molar ratios equal to 0.3 and 0.1, respectively) was selected for OSR experiments. Thus, a prevalence of methane dry reforming with respect to steam and partial/total oxidation of methane can be predicted. At 800 °C (Fig. 8a), Ni–MO catalysts showed almost constant catalytic activity in all the investigated WSV range, leading to CH_4 and CO_2 conversion of 98.5 and 87.2%, respectively, at WSV of 70,000 Nml g_{cat}^{-1} h^{-1}. However, a slight decrease down to 91.1% (CH_4 conversion) and 82.3% (CO_2 conversion) was evidenced at high space velocity. An almost constant H_2/CO molar ratio (1.34–1.36) was also recorded. At 700 °C (Fig. 8b), catalytic activity rapidly decreased with increasing space velocity: CH_4 and CO_2 conversions were 50.0 and 36.4, respectively, at WSV of 350,000 Nml g_{cat}^{-1} h^{-1}. In addition, H_2/CO molar ratio (1.41–1.55) was always lower than equilibrium values calculated at T_{SET} of 700 °C, probably due to the higher T_{IN} and T_{OUT}. Moreover, the occurrence of reverse water gas shift reaction (RWGS) cannot be excluded [58].

It is widely reported [59,60] that syngas production by reforming reactions in presence of oxygen proceeds by a two steps path: (i) methane combustion that produces H_2O and CO_2, followed by (ii) methane reforming reactions (with H_2O and CO_2) that produce syngas. Besides, in the first part of the catalytic bed, partial oxidation of nickel species (with high activity for combustion reaction) occurs [61]. After total oxygen oxidation, in the second part of the bed reforming reactions prevail. The good balance between the oxidation-reforming zones determines catalyst reforming activity. The occurrence of oxidation zone could be confirmed by the high temperature that was recorded as T_{IN}, while the high recorded temperature at the exit of the catalytic bed (T_{OUT}) is due to the heat provided by the furnace for supporting endothermic steam and dry reforming reactions [34,59,60].

3.3.2. *Effect of catalytic formulation and support geometry on the SR and OSR activity*

The catalytic activity of Ni–MO, NiRh–MO and NiRh–FO systems was investigated towards biogas SR (Table 3) and OSR (Table 4), at

different temperatures (700–800 °C) and weight space velocities (WSV = 250,000–350,000 Nml g_{cat}^{-1} h^{-1}). The comparative analysis of catalytic performance in biogas SR and OSR gave information about catalytic formulation effect on activity. NiRh-based catalyst showed slightly better performance than Ni-based catalyst, especially at low temperatures. This was due to (i) the higher loading of active ingredients in the catalytic formulation and (ii) Rh promoter effect, as reported by several authors [9,21,22].

Meanwhile, from the point of view of catalyst geometry, both monolith and foam are promising for efficient structured catalysts manufacturing for biogas reforming into syngas. Catalytic activity tests showed that foam structured catalysts allowed higher activity with respect to honeycomb structured catalysts. As reported by Ciambelli at al. [29], the random porous network of a foam catalyst carrier may determine an improvement in gas temperature profile and species diffusion. Therefore, the higher performance of Ni–Rh-foam structured system as compared with the same active component on monolith could be explained by the presence of a more efficient mass transfer, making the catalytic phase more accessible to reagents.

4. Conclusions

In this work, structured ceramic honeycomb monolith and open cell foam were employed as Ni(7.5 wt.%)/CeO_2 and Ni(7.5 wt.%)-Rh(0.5 wt.%)/CeO_2 catalysts support for biogas steam reforming and oxy-steam reforming reactions. Catalytic powders (previously prepared by solution combustion synthesis) were washcoated by means of support dip-coating into acid-free catalyst dispersion. A catalysts comparative analysis was reported on the basis of their performance in different operating conditions (reactants mixture composition, temperature and space velocity), highlighting the effect of catalytic formulation and support geometry on activity towards reforming processes.

Coating load was controlled by multiple depositions depending on the sample, or, more precisely, on slurry rheological behavior and on support geometry. Homogeneous and well adherent layers of ca. 20–30 μm were found.

Good catalytic activity was obtained on Ni/CeO_2-based structured catalysts, but it decreased with increasing space velocity. NiRh-based catalysts showed slightly better performance than Ni-based systems, especially at low temperatures and high space velocity, mainly due to Rh promoter effect. Regarding the catalyst geometry, both monolith and foam were found to be promising for efficient structured catalysts manufacturing for biogas reforming into syngas. The higher performance of foam supported Ni-Rh catalyst was explained by more efficient heat and mass transfer phenomena, due to the random porous network of foam support.

Acknowledgements

This work was funded by the Italian Ministry of Education, University and Research (MIUR, Progetti di Ricerca Scientifica di Rilevante Interesse Nazionale 2010–2011) within the project IFOAMS ("*Intensification of catalytic processes for clean energy, low-emission transport and sustainable chemistry using open-cell FOAMS as novel advanced structured materials*", protocol no. 2010XFT2BB).

References

[1] L.B. Braga, J.L. Silveira, M.E. da Silva, C.E. Tuna, E.B. Machin, D.T. Pedroso, Hydrogen production by biogas steam reforming: a technical, economic and ecological analysis, Renew. Sust. Energy Rev. 28 (2013) 166–173.
[2] S. Ahmed, M. Krumpelt, Hydrogen from hydrocarbon fuels for fuel cells, Int. J. Hydrogen Energy 26 (2001) 291–301.
[3] S. Dunn, Hydrogen futures: toward a sustainable energy system, Int. J. Hydrogen Energy 27 (2002) 235–264.
[4] P.P. Edwards, V.L. Kuznetsov, W.I.F. David, Hydrogen energy, Philos. Trans. Math. Phys. Eng. Sci. 365 (2007) 1043–1056.
[5] S. Specchia, Fuel processing activities at European level: a panoramic overview, Int. J. Hydrogen Energy 39 (2014) 17953–17968.
[6] J. Xu, W. Zhou, Z. Li, J. Wang, J. Ma, Biogas reforming for hydrogen production over nickel and cobalt bimetallic catalysts, Int. J. Hydrogen Energy 34 (2009) 6646–6654.
[7] M. Ashrafi, T. Pröll, C. Pfeifer, H. Hofbauer, Experimental study of model biogas catalytic steam reforming: 1. Thermodynamic optimization, Energy Fuels 22 (2008) 4182–4189.
[8] J. Maney, Carbon dioxide emissions, climate change, and the clean air act: An analysis of whether carbon dioxide should be listed as a criteria pollutant, N.Y.U. Environ. Law J. 13 (2005) 298–373.
[9] U. Izquierdo, V.L. Barrio, N. Lago, J. Requies, J.F. Cambra, M.B. Güemez, P.L. Arias, Biogas steam and oxidative reforming processes for synthesis gas and hydrogen production in conventional and microreactor reaction systems, Int. J. Hydrogen Energy 37 (2012) 13829–13842.
[10] U. Izquierdo, V.L. Barrio, J. Requies, J.F. Cambra, M.B. Güemez, P.L. Arias, Tri-reforming: A new biogas process for synthesis gas and hydrogen production, Int. J. Hydrogen Energy 38 (2013) 7623–7631.
[11] S. Araki, N. Hino, T. Mori, S. Hikazudani, Durability of a Ni based monolithic catalyst in the autothermal reforming of biogas, Int. J. Hydrogen Energy 34 (2009) 4727–4734.
[12] K. Tomishige, M. Asadullah, K. Kunimori, Syngas production by biomass gasification using Rh/CeO_2/SiO_2 catalysts and fluidized bed reactor, Catal. Today 89 (2004) 389–403.
[13] K. Kusakabe, K.-I. Sotowa, T. Eda, Y. Iwamoto, Methane steam reforming over Ce-ZrO2-supported noble metal catalysts at low temperature, Fuel Process. Technol. 86 (2004) 319–326.
[14] M. Nurunnabi, B. Li, K. Kunimori, K. Suzuki, K.-I. Fujimoto, K. Tomishige, Performance of NiO–MgO solid solution-supported Pt catalysts in oxidative steam reforming of methane, Appl. Catal. A 292 (2005) 272–280.
[15] B.C. Michael, A. Donazzi, L.D. Schmidt, Effects of H_2O and CO_2 addition in catalytic partial oxidation of methane on Rh, J. Catal. 265 (2009) 117–129.
[16] N. Laosiripojana, S. Assabumrungrat, Methane steam reforming over Ni/Ce–ZrO_2 catalyst: Influences of Ce–ZrO_2 support on reactivity, resistance toward carbon formation, and intrinsic reaction kinetics, Appl. Catal. A 290 (2005) 200–211.
[17] T.-J. Huang, T.-C. Yu, Effect of steam and carbon dioxide pretreatments on methane decomposition and carbon gasification over doped-ceria supported nickel catalyst, Catal. Letters 102 (2005) 175–181.
[18] A. Vita, C. Italiano, C. Fabiano, M. Laganà, L. Pino, Influence of Ce-precursor and fuel on structure and catalytic activity of combustion synthesized Ni/CeO_2 catalysts for biogas oxidative steam reforming, Mater. Chem. Phys. 163 (2015) 337–347.
[19] K.-H. Lin, H.-F. Chang, A.C.C. Chang, Biogas reforming for hydrogen production over mesoporous $Ni_{2x}Ce_{1-x}O2$ catalysts, Int. J. Hydrogen Energy 37 (2012) 15696–15703.
[20] C. Italiano, A. Vita, C. Fabiano, M. Laganà, L. Pino, Bio-hydrogen production by oxidative steam reforming of biogas over nanocrystalline Ni/CeO_2 catalysts, Int. J. Hydrogen Energy 40 (2015) 11823–11830.
[21] V.A. Tsipouriari, A.M. Efstathiou, Z.L. Zhang, X.E. Verykios, Reforming of methane with carbon dioxide to synthesis gas over supported Rh catalysts, Catal. Today 21 (1994) 579–587.
[22] Y.-G. Chen, K. Tomishige, K. Yokoyama, K. Fujimoto, Promoting effect of Pt, Pd and Rh noble metals to the $Ni_{0.03}Mg_{0.97}O$ solid solution catalysts for the reforming of CH_4 with CO_2, Appl. Catal. A 165 (1997) 335–347.
[23] S. Specchia, A. Civera, G. Saracco, In situ combustion synthesis of perovskite catalysts for efficient and clean methane premixed metal burners, Chem. Eng. Sci. 59 (2004) 5091–5098.
[24] S.R. Jain, K.C. Adiga, V.R. Pai Verneker, A new approach to thermochemical calculations of condensed fuel-oxidizer mixtures, Combust. Flame 40 (1981) 71–79.
[25] R.D. Purohit, B.P. Sharma, K.T. Pillai, A.K. Tyagi, Ultrafine ceria powders via glycine-nitrate combustion, Mater. Res. Bull. 36 (2001) 2711–2721.
[26] W. Chen, F. Li, J. Yu, Combustion synthesis and characterization of nanocrystalline CeO_2-based powders via ethylene glycol-nitrate process, Mater. Lett. 60 (2006) 57–62.
[27] V. Sadykov, L. Bobrova, S. Pavlova, V. Simagina, L. Makarshin, V. Parmon, J.R.H. Ross, A.C. Van Veen, C. Mirodatos, Syngas Generation from Hydrocarbons and Oxygenates with Structured Catalysts, Nova Science Publishers Inc., New York, 2012.
[28] M.E. Domine, E.E. Iojoiu, T. Davidian, N. Guilhaume, C. Mirodatos, Hydrogen production from biomass-derived oil over monolithic Pt- and Rh-based catalysts using steam reforming and sequential cracking processes, Catal. Today 133-135 (2008) 565–573.
[29] P. Ciambelli, V. Palma, E. Palo, Comparison of ceramic honeycomb monolith and foam as Ni catalyst carrier for methane autothermal reforming, Catal. Today 155 (2010) 92–100.
[30] V. Sadykov, V. Sobyanin, N. Mezentseva, G. Alikina, Z. Vostrikov, Y. Fedorova, V. Pelipenko, V. Usoltsev, S. Tikhov, A. Salanov, L. Bobrova, S. Beloshapkin, J.R.H. Ross, O. Smorygo, V. Ulyanitskii, V. Rudnev, Transformation of CH_4 and liquid fuels into syngas on monolithic catalysts, Fuel 89 (2010) 1230–1240.
[31] O. Smorygo, V. Sadykov, V. Mikutski, A. Marukovich, A. Ilyushchanka, A. Yarkovich, N. Mezentseva, L. Bobrova, Y. Fedorova, V. Pelipenko, M. Arapova,

A. Smirnova, Porous substrates for intermediate temperature SOFCs and in-cell reforming catalysts, Catal. Sustain. Energy 1 (2013) 90–99.
[32] V. Palma, A. Ricca, P. Ciambelli, Methane auto-thermal reforming on honeycomb and foam structured catalysts: the role of the support on system performances, Catal. Today 216 (2013) 30–37.
[33] V. Sadykov, N. Mezentseva, Y. Fedorova, A. Lukashevich, V. Pelipenko, V. Kuzmin, M. Simonov, A. Ishchenko, Z. Vostrikov, L. Bobrova, E. Sadovskaya, V. Muzykantov, A. Zadesenets, O. Smorygo, A.C. Roger, K. Parkhomenko, Structured catalysts for steam/autothermal reforming of biofuels on heat-conducting substrates: design and performance, Catal. Today 251 (2015) 19–27.
[34] A. Vita, G. Cristiano, C. Italiano, L. Pino, S. Specchia, Syngas production by methane Oxy-steam reforming on Me/CeO_2 (Me = Rh, Pt Ni) catalyst lined on cordierite monoliths, Appl. Catal. B 162 (2015) 551–563.
[35] V. Meille, Review on methods to deposit catalysts on structured surfaces, Appl. Catal. A 315 (2006) 1–17.
[36] O. Sanz, F.J. Echave, F. Romero-Sarria, J.A. Odriozola, M. Montes, Chapter 9—advances in structured and microstructured catalytic reactors for hydrogen production, in: L.M.G.A.M. Diéguez (Ed.), Renewable Hydrogen Technologies, Elsevier, Amsterdam, 2013, pp. 201–224.
[37] E.D. Banús, V.G. Milt, E.E. Miró, M.A. Ulla, Catalytic coating synthesized onto cordierite monolith walls. Its application to diesel soot combustion, Appl. Catal. B 132-133 (2013) 479–486.
[38] P. Avila, M. Montes, E.E. Miro, Monolithic reactors for environmental applications – A review on preparation technologies, Chem. Eng. J. 109 (2005) 11–36.
[39] A. Montebelli, C.G. Visconti, G. Groppi, E. Tronconi, C. Cristiani, C. Ferreira, S. Kohler, Methods for the catalytic activation of metallic structured substrates, Catal. Sci. Technol. 4 (2014) 2846–2870.
[40] S. Middleman, Fundamentals of Polymers Processing, McGraw-Hill Companies, New York, 1977.
[41] C.J. Brinker, G.W. Scherer, Sol–Gel Science, Academic Press, San Diego, 1990.
[42] M. Valentini, G. Groppi, C. Cristiani, M. Levi, E. Tronconi, P. Forzatti, The deposition of-Al2O3 layers on ceramic and metallic supports for the preparation of structured catalysts, Catal. Today 69 (2001) 307–314.
[43] R. Balzarotti, C. Cristiani, S. Latorrata, A. Migliavacca, Washcoating of low surface area cerium oxide on complex geometry substrates, Part. Sci. Technol. (2015) null–null.
[44] C. Cristiani, E. Finocchio, S. Latorrata, C.G. Visconti, E. Bianchi, E. Tronconi, G. Groppi, P. Pollesel, Activation of metallic open-cell foams via washcoat deposition of $Ni/MgAl_2O_4$ catalysts for steam reforming reaction, Catal. Today 197 (2012) 256–264.
[45] A. Montebelli, C.G. Visconti, G. Groppi, E. Tronconi, S. Kohler, H.J. Venvik, R. Myrstad, Washcoating and chemical testing of a commercial $Cu/ZnO/Al_2O_3$ catalyst for the methanol synthesis over copper open-cell foams, Appl. Catal. A 481 (2014) 96–103.
[46] L. Pino, A. Vita, F. Cipitì, M. Laganà, V. Recupero, Hydrogen production by methane tri-reforming process over Ni-ceria catalysts: effect of La-doping, Appl. Catal. B 104 (2011) 64–73.
[47] J. Xiaoyuan, L. Guanglie, Z. Renxian, M. Jianxin, C. Yu, Z. Xiaoming, Studies of pore structure temperature-programmed reduction performance, and micro-structure of CuO/CeO_2 catalysts, Appl. Surf. Sci. 173 (2001) 208–220.
[48] J. Kugai, S. Velu, C. Song, Low-temperature reforming of ethanol over CeO_2-supported Ni–Rh bimetallic catalysts for hydrogen production, Catal. Lett. 101 (2005) 255–264.
[49] T. Hou, B. Yu, S. Zhang, T. Xu, D. Wang, W. Cai, Hydrogen production from ethanol steam reforming over Rh/CeO_2 catalyst, Catal. Commun. 58 (2015) 137–140.
[50] F. Menegazzo, M. Signoretto, F. Pinna, P. Canton, N. Pernicone, Optimization of bimetallic dry reforming catalysts by temperature programmed reaction, Appl. Catal. A 439–440 (2012) 80–87.
[51] J. Kugai, V. Subramani, C. Song, M.H. Engelhard, Y.-H. Chin, Effects of nanocrystalline CeO_2 supports on the properties and performance of Ni–Rh bimetallic catalyst for oxidative steam reforming of ethanol, J. Catal. 238 (2006) 430–440.
[52] F.C. Patcas, G.I. Garrido, B. Kraushaar-Czarnetzki, CO oxidation over structured carriers: a comparison of ceramic foams, honeycombs and beads, Chem. Eng. Sci. 62 (2007) 3984–3990.
[53] J.L. Williams, Monolith structures materials, properties and uses, Catal. Today 69 (2001) 3–9.
[54] L.J. Gibson, F. Ashby, Cellular Solids Structure and Properties, University Press, Cambridge, 1999.
[55] A. Cybulski, J.A. Moulijn, Monoliths in heterogeneous catalysis, Catal. Rev. 36 (1994) 179–270.
[56] F.C. Buciuman, B. Kraushaar-Czarnetzki, Ceramic foam monoliths as catalyst carriers. 1. Adjustment and description of the morphology, Ind. Eng. Chem. Res. 42 (2003) 1863–1869.
[57] S.D. Angeli, L. Turchetti, G. Monteleone, A.A. Lemonidou, Catalyst development for steam reforming of methane and model biogas at low temperature, Appl. Catal. B 181 (2016) 34–46.
[58] P.S. Roy, C.S. Park, A.S.K. Raju, K. Kim, Steam-biogas reforming over a metal-foam-coated $(Pd–Rh)/(CeZrO_2–Al_2O_3)$ catalyst compared with pellet type alumina-supported Ru and Ni catalysts, J. CO_2 Util. 12 (2015) 12–20.
[59] K. Tomishige, S. Kanazawa, K. Suzuki, M. Asadullah, M. Sato, K. Ikushima, K. Kunimori, Effective heat supply from combustion to reforming in methane reforming with CO_2 and O_2: comparison between Ni and Pt catalysts, Appl. Catal. A 233 (2002) 35–44.
[60] K. Tomishige, M. Nurunnabi, K. Maruyama, K. Kunimori, Effect of oxygen addition to steam and dry reforming of methane on bed temperature profile over Pt and Ni catalysts, Fuel Process. Technol. 85 (2004) 1103–1120.
[61] F. van Looij, J.W. Geus, Nature of the active phase of a nickel catalyst during the partial oxidation of methane to synthesis gas, J. Catal. 168 (1997) 154–163.